Canonical maximization of coherence

NeuroImage 201 (2019) 116009

Contents lists available at ScienceDirect

NeuroImage

journal homepage: www.elsevier.com/locate/neuroimage

Canonical maximization of coherence: A novel tool for investigation of neuronal interactions between two datasets

C. Vidaurre [a,b,*], G. Nolte [c], I.E.J. de Vries [d], M. Gómez [a], T.W. Boonstra [e,f], K.-R. Müller [b,g,h], A. Villringer [i,k], V.V. Nikulin [i,j,l,**]

[a] Dept of Statistics, Informatics and Mathematics, Public University of Navarre, Pamplona, Spain
[b] Machine Learning Group, EE & Computer Science Faculty, TU-Berlin, Germany
[c] Dept. of Neurophysiology and Pathophysiology, University Medical Center Hamburg-Eppendorf, Hamburg, Germany
[d] Faculty of Behavioural and Movement Sciences, Dept. of Experimental and Applied Psychology, Vrije Universiteit Amsterdam, the Netherlands
[e] Faculty of Psychology and Neuroscience, Dept. of Neuropsychology and Psychopharmacology, Maastricht University, Maastricht, the Netherlands
[f] Neuroscience Research Australia, Sydney, Australia
[g] Department of Brain and Cognitive Engineering, Korea University, Seoul, South Korea
[h] Max Planck Institute for Informatics, Saarbrücken, Germany
[i] Department of Neurology, Max Planck Institute for Human Cognitive and Brain Sciences, Leipzig, Germany
[j] Institute for Cognitive Neuroscience, National Research University Higher School of Economics, Russian Federation
[k] Berlin School of Mind and Brain, Humboldt-Universität zu Berlin, Berlin, Germany
[l] Neurophysics Group, Department of Neurology, Campus Benjamin Franklin, Charité-Universitätsmedizin Berlin, Berlin, Germany

ARTICLE INFO

Keywords:
Coherence optimization
Multivariate methods
Multimodal methods
Cortico-muscular coherence (CMC)
Electroencephalography (EEG)
Electromyography (EMG)
High density electromyography (HDsEMG)
Magnetoencephalography (MEG)
Local field potentials (LFP)

ABSTRACT

Synchronization between oscillatory signals is considered to be one of the main mechanisms through which neuronal populations interact with each other. It is conventionally studied with mass-bivariate measures utilizing either sensor-to-sensor or voxel-to-voxel signals. However, none of these approaches aims at maximizing synchronization, especially when two multichannel datasets are present. Examples include cortico-muscular coherence (CMC), cortico-subcortical interactions or hyperscanning (where electroencephalographic EEG/magnetoencephalographic MEG activity is recorded simultaneously from two or more subjects). For all of these cases, a method which could find two spatial projections maximizing the strength of synchronization would be desirable. Here we present such method for the maximization of coherence between two sets of EEG/MEG/EMG (electromyographic)/LFP (local field potential) recordings. We refer to it as canonical Coherence (caCOH). caCOH maximizes the absolute value of the coherence between the two multivariate spaces in the frequency domain. This allows very fast optimization for many frequency bins. Apart from presenting details of the caCOH algorithm, we test its efficacy with simulations using realistic head modelling and focus on the application of caCOH to the detection of cortico-muscular coherence. For this, we used diverse multichannel EEG and EMG recordings and demonstrate the ability of caCOH to extract complex patterns of CMC distributed across spatial and frequency domains. Finally, we indicate other scenarios where caCOH can be used for the extraction of neuronal interactions.

1. Introduction

Effective estimation of synchrony between oscillatory neuronal signals is of key importance in neuroscience. Previous research on cortical processing has shown that phase synchronization is a prerequisite for effective communication between neuronal populations (Fries, 2005), providing large-scale integration (Varela et al., 2001) and selection of perceptually and behaviorally relevant information (Engel et al., 1997). Large-scale synchronization is not restricted to the cortical level, as previous studies have shown that it is also an effective way for the communication between cortex and spinal cord (Baker et al., 1997; Schoffelen et al., 2005; Bayraktaroglu et al., 2011). In particular, cortical oscillations at beta frequency range (15–30 Hz) have been implicated in different aspects of the motor control (Donoghue et al., 1998; Murthy and

* Corresponding author. Dept of Statistics, Informatics and Mathematics, Public University of Navarre, Pamplona, Spain.
** Corresponding author. Department of Neurology, Max Planck Institute for Human Cognitive and Brain Sciences, Leipzig, Germany.
E-mail addresses: carmen.vidaurre@unavarra.es (C. Vidaurre), nikulin@cbs.mpg.de (V.V. Nikulin).

https://doi.org/10.1016/j.neuroimage.2019.116009
Received 15 February 2019; Received in revised form 24 May 2019; Accepted 10 July 2019
Available online 11 July 2019

Fetz, 1992; Penfield, 1954). In this respect, cortico-muscular coherence (CMC) provides a unique possibility to investigate in a non-invasive way the coupling between sensorimotor cortices and muscle activity (Baker, 2007; Jackson et al., 2002; Schnitzler et al., 2000).

CMC measures synchronization between cortical and muscular activities at specific frequency bands. Its magnitude is particularly strong during isometric parts of the movement whereas it decreases during kinematically active parts (Kilner et al., 2000a; Riddle and Baker, 2005a). The peak of CMC generally has a maximum in the beta frequency range (15–30 Hz) over the primary sensorimotor cortices contralateral to the limb (Salenius et al., 1997; Tsujimoto et al., 2009; Witham et al., 2010; Steeg et al., 2014). In healthy subjects, CMC has been mainly assessed during isometric muscle contractions in experiments in which cortical activity was non-invasively recorded with magnetoencephalography (MEG) (Conway et al., 1995; Salenius et al., 1997) as well as with electroencephalography (EEG) (Baker and Baker, 2002; Graziadio et al., 2010; Halliday et al., 1998; Kristeva-Feige et al., 2002; Mima and Hallett, 1999). CMC has also been assessed in experiments performed in monkeys where intracortical local field potentials (LFP) were acquired (Baker et al., 1997). Different studies have reported maximum values of CMC ranging between 0.02 and 0.2 (Conway et al., 1995; Riddle and Baker, 2005b; Salenius and Hari, 2003), and certain parameters such as peak frequency, spectral distribution and magnitude are thought to be modulated by task, attention and age (Graziadio et al., 2010; Kristeva--Feige et al., 2002; Riddle and Baker, 2005a).

Because of its weak strength as well as distributed cortical origin, detection of CMC remains challenging and thus further methodological improvements are necessary. For example, we presented a procedure to maximize CMC called rCMC (Bayraktaroglu et al., 2011). In that paper, CMC between a set of EEG sensors (multivariate subspace) and one electromyographic (EMG) electrode (univariate subspace) was optimized. rCMC is a parametric model based on multiple regression. The delay between EEG and EMG and the frequency band of interest are searched until the linear combination of band-pass filtered EEG signals (independent variables) that maximize CMC, using the EMG electrode as dependent variable, is found. We demonstrated that rCMC returns significantly higher CMC values than CMC computed between Laplacian derivations of EEG channels and the EMG electrode. This last approach is commonly used in CMC studies (Andrykiewicz et al., 2007; Graziadio et al., 2010; Mima and Hallett, 1999; Saglam et al., 2008). rCMC also allows obtaining the spatial pattern (source) of electrical brain signals associated to the maximum CMC. Yet, rCMC is not capable of taking into account the fact that cortico-spinal interactions are multivariate in nature, not only on the cortical level, but also at the level of the spinal cord, where multiple afferent and efferent processes occur, thus leading to intricate patterns of muscle activity. For example, CMC can be assessed using an electrode grid placed over the muscle (high-density EMG), (Steeg et al., 2014). This can only be achieved with a algorithm that maximizes synchronization taking into account multivariate central (EEG/MEG) and peripheral (EMG) signals.

In this paper we present a method to maximize coherence between a set of EEG electrodes and another set of EMG electrodes. This technique is called canonical Coherence (caCOH) and is a generalization of rCMC because both subspaces are multivariate. Unlike rCMC, which relies on optimization in the time domain, caCOH directly maximizes the absolute value of the coherence between two multivariate spaces in the frequency domain. This allows very fast optimization for multiple frequency bins. Thus, it is possible to study CMC within wider frequency ranges and different delays.

Apart from presenting the method, we demonstrate its efficacy with extensive simulations on the basis of realistic head modelling and show its application for empirical multi-channel EEG and EMG recordings. Finally, we provide other examples where caCOH can be used for the investigation of paired datasets, for instance in case of cortico-subcortical interactions and for hyperscanning. As caCOH maximizes a magnitude computed from signals belonging to different modalities, it is related to the multi-modal signal processing field. This field has experienced a great advancement over the last years. Some examples of new multimodal procedures are summarized in (Calhoun et al., 2009; Bießmann et al., 2010, 2011; Dähne et al., 2015), where signals are mostly treated in time domain. In contrast, in this manuscript we introduce a new multimodal method for the frequency domain.

2. Methods

2.1. Theoretical description of canonical coherence (caCOH)

caCOH maximizes the absolute value of coherence between two spaces A and B of dimension N_A and N_B, respectively. In our case, A is the set of N_a vectors of signals from EMG sensors and B is the set of N_B vectors of signals from EEG sensors. The goal is to find a real valued linear combination of vectors of A and a real valued linear combination of vectors of B such that the absolute value of coherence between the two virtual sensors (i.e projected data) is maximized at a specific frequency. Please, note that the linear combination of vectors are real valued because an instantaneous mixing of the signals of spaces A and respectively B is assumed. We first write the cross-spectrum between all sensors (i.e. sets A and B combined) as a block matrix

$$\mathbf{C} = \begin{pmatrix} \mathbf{C}_{AA} & \mathbf{C}_{AB} \\ \mathbf{C}_{BA} & \mathbf{C}_{BB} \end{pmatrix} \tag{1}$$

As aforementioned, our aim is now to find real valued column vectors $\boldsymbol{\alpha}$ and $\boldsymbol{\beta}$ of size N_A and N_B, respectively, such that

$$L(\boldsymbol{\alpha}, \boldsymbol{\beta}) = \frac{\left|\boldsymbol{\alpha}^T \mathbf{C}_{AB} \boldsymbol{\beta}\right|^2}{\boldsymbol{\alpha}^T \mathbf{C}_{AA} \boldsymbol{\alpha} \boldsymbol{\beta}^T \mathbf{C}_{BB} \boldsymbol{\beta}} \tag{2}$$

is maximized. Note that L (square of absolute value of coherence) is a fourth order function of the parameters that cannot be analytically optimized. Thus, it must be maximized numerically. We here propose a procedure that reduces this optimization to a numerical optimization over a single parameter, the phase lag between the two spaces A and B. In order to achieve it, we require analytic techniques used to optimize the real part of the coherence, which will be applied below to a transformed cross-spectrum. Let us first write the (complex) coherence in polar coordinates

$$\frac{\boldsymbol{\alpha}^T \mathbf{C}_{AB} \boldsymbol{\beta}}{\sqrt{\boldsymbol{\alpha}^T \mathbf{C}_{AA} \boldsymbol{\alpha} \boldsymbol{\beta}^T \mathbf{C}_{BB} \boldsymbol{\beta}}} = \exp(i\Phi) c \tag{3}$$

where c is the absolute value of coherence (a real valued number). Thus:

$$c = \frac{\boldsymbol{\alpha}^T \exp(-i\Phi) \mathbf{C}_{AB} \boldsymbol{\beta}}{\sqrt{\boldsymbol{\alpha}^T \mathbf{C}_{AA} \boldsymbol{\alpha} \boldsymbol{\beta}^T \mathbf{C}_{BB} \boldsymbol{\beta}}} \tag{4}$$

The denominator of Equation (4) is real since $\boldsymbol{\alpha}$ and $\boldsymbol{\beta}$ are real valued vectors and the cross-spectral matrices $\mathbf{C}_{AA}$ and $\mathbf{C}_{BB}$ are Hermitian. Note also that, in order to obtain a real value c, and taking into account that $\boldsymbol{\alpha}$ and $\boldsymbol{\beta}$ are real-valued, one necessarily needs to take $\Re(\exp(-i\Phi)\mathbf{C}_{AB})$ to reach the desired real solution. Thus, with $\Re(\cdot)$ denoting real part, the last equation is equivalent to:

$$L_R(\Phi)^{1/2} = c = \frac{\boldsymbol{\alpha}^T \Re(\exp(-i\Phi)\mathbf{C}_{AB})\boldsymbol{\beta}}{\sqrt{\boldsymbol{\alpha}^T \mathbf{C}_{AA} \boldsymbol{\alpha} \boldsymbol{\beta}^T \mathbf{C}_{BB} \boldsymbol{\beta}}} \tag{5}$$

Therefore, if we know the phase of the coherence with maximal absolute value we can find the vectors $\boldsymbol{\alpha}$ and $\boldsymbol{\beta}$ that maximize $L(\Phi)$. Since we do not know the phase, we make a nonlinear search across all phases. That must be done numerically, but it is only a one-dimensional maximization over a finite range of the parameter Φ. On the other hand, the analytic maximization of Equation (5) is standard and equivalent to an eigenvalue problem, but we will here recall the steps. Let the absolute

value of coherence be:

$$L_R(\boldsymbol{\alpha},\boldsymbol{\beta},\Phi)^{1/2} = \frac{\boldsymbol{\alpha}^T \mathbf{C}^R_{AB,\Phi}\boldsymbol{\beta}}{\sqrt{\boldsymbol{\alpha}^T \mathbf{C}_{AA}\boldsymbol{\alpha}\boldsymbol{\beta}^T \mathbf{C}_{BB}\boldsymbol{\beta}}} \tag{6}$$

where $\mathbf{C}^R_{AB,\Phi}$ denotes the real part of the cross-spectrum $\exp(-i\Phi)\mathbf{C}_{AB}$. Since the cross-spectral matrices are Hermitian, the respective imaginary parts of $\mathbf{C}_{AA}$ and $\mathbf{C}_{BB}$ are irrelevant. Thus, we implicitly understand that these imaginary parts are set to zero without changing notation here. Now we make a change of coordinates and define

$$\begin{aligned}\mathbf{a} &= \mathbf{C}^{1/2}_{AA}\boldsymbol{\alpha}\\ \mathbf{b} &= \mathbf{C}^{1/2}_{BB}\boldsymbol{\beta}\end{aligned} \tag{7}$$

Then $L_R^{1/2}$ becomes

$$L_R(\mathbf{a},\mathbf{b},\Phi)^{1/2} = \frac{\mathbf{a}^T\mathbf{D}(\Phi)\mathbf{b}}{\sqrt{\mathbf{a}^T\mathbf{a}\mathbf{b}^T\mathbf{b}}} \tag{8}$$

with

$$\mathbf{D}(\Phi) = \mathbf{C}^{-1/2}_{AA}\mathbf{C}^R_{AB,\Phi}\mathbf{C}^{-1/2}_{BB} \tag{9}$$

Calculating the derivative of $L_R(\mathbf{a},\mathbf{b},\Phi)$ with respect to the components of $\mathbf{a}$ and $\mathbf{b}$ and setting that to zero leads to

$$\mathbf{D}(\Phi)\mathbf{b} = \frac{\mathbf{a}^T\mathbf{D}(\Phi)\mathbf{b}}{\mathbf{a}^T\mathbf{a}}\mathbf{a} \tag{10}$$

$$\mathbf{D}(\Phi)^T\mathbf{a} = \frac{\mathbf{a}^T\mathbf{D}(\Phi)\mathbf{b}}{\mathbf{b}^T\mathbf{b}}\mathbf{b} \tag{11}$$

Multiplying Equation (10) with $\mathbf{D}(\Phi)^T$ and using Equation (11), and multiplying Equation (11) with $\mathbf{D}(\Phi)$ and using Equation (10), leads to the following eigenvalue problem

$$\begin{aligned}\mathbf{D}(\Phi)^T\mathbf{D}(\Phi)\mathbf{b} &= \lambda\mathbf{b}\\ \mathbf{D}(\Phi)\mathbf{D}(\Phi)^T\mathbf{a} &= \lambda\mathbf{a}\end{aligned} \tag{12}$$

with

$$\lambda(\Phi) = L(\Phi) = \frac{(\mathbf{a}^T\mathbf{D}(\Phi)\mathbf{b})^2}{\mathbf{a}^T\mathbf{a}\mathbf{b}^T\mathbf{b}} \tag{13}$$

being the square of the coherence. The vectors $\boldsymbol{\alpha}$ and $\boldsymbol{\beta}$ can be reconstructed from the eigenvector $\mathbf{a}$ and $\mathbf{b}$ using Equation (7), where $\lambda(\Phi)$, respectively $L(\Phi)$ is the maximal eigenvalue of Equation (12). To maximize $L(\Phi)$ we first evaluate it over 5 different values of Φ in the range $[\pi/5, \pi]$ and pick the maximizing Φ. Then, we iteratively make a second order Taylor expansion around the present value of Φ, calculating first and second derivative numerically, and maximize the corresponding quadratic function with an adaptive step size as used in the Levenberg-Marquardt algorithm. A total of 10 iterations is sufficient to arrive at an essentially exact solution.

Finally, in order to find the topographies corresponding to the spatial filters $\boldsymbol{\alpha}$ and $\boldsymbol{\beta}$, one needs multiply the filters with their respective real part of the cross-spectral matrix, that is:

$$\begin{aligned}t_\alpha &= \mathbf{C}^R_{AA}\boldsymbol{\alpha}\\ t_\beta &= \mathbf{C}^R_{BB}\boldsymbol{\beta}\end{aligned} \tag{14}$$

Please, note that these topographies correspond to the *patterns of the sources of maximal coherence*. The time courses of caCOH components directly show activity of neuronal sources. However, the exact spatial location of these sources in the brain should be recovered with source modelling using the obtained caCOH patterns as in Equation (14). caCOH topographies are different from the usual patterns of coherence that only offer information about the distribution of coherence on the scalp, but not about its neural sources. Often coherence is recovered using source modelling and then multiple calculations are necessary for all the recovered sources. In contrast, caCOH directly finds topographies of only those neuronal sources that are coupled to maximal coherence.

In order to obtain the results presented in this manuscript, we computed cross-spectra using the Fast-Fourier Transform algorithm (FFT). The parameters employed were: window length of 2 s, a Hanning window and 50% overlap and a sampling frequency of 200 Hz (therefore the frequency resolution was 0.5 Hz).

2.2. Overfitting

The filters $\boldsymbol{\alpha}$ and $\boldsymbol{\beta}$ in section 2.1 are computed such that caCOH is maximized. However, the spatial filters might overfit, that is, they might not be generalizable to new data. To overcome this problem one can reduce the dimensionality of the real part of the cross-spectra in the spaces A and B, at each frequency bin, and before computing spatial filters. For that, we used the singular value decomposition (SVD) and selected singular vectors in each of the two data spaces whose singular values retained at least 99% of the information. If $\mathbf{C}^R$ is the frequency dependent real part of the cross-spectrum, the SVD is such that:

$$\mathbf{C}^R = \mathbf{U}\boldsymbol{\Sigma}\mathbf{V}^T \tag{15}$$

Now, the real part of the cross-spectrum is reduced by choosing column wise the first p components of the matrix $\mathbf{U} \in \mathbb{R}^{nxn}$. The cross-spectrum can be projected onto a lower dimensional space by $\mathbf{C}^R = U^T\mathbf{C}U$ with $\mathbf{C}^R \in \mathbb{R}^{pxp}$.

2.3. Simulations

We performed simulations in order to test the ability of caCOH to maximize CMC. In particular, we studied whether caCOH is able to obtain spatial filters that maximize coherence between several EMG channels and their corresponding coupled neuronal source. We estimated CMC using two different methods: Laplacian CMC between pairs of EEG-EMG channels and caCOH. We simulated two different EEG sources coupled with their corresponding EMG sources, each of them at a different frequency, while cortical sources were not coupled between each other. We additionally included strong background noise in the generation of both EEG and EMG signals with variable signal-to-noise ratios (SNR). The EEG signals were simulated for 61 channels, fitted to the outermost layer of the standard Montreal Neurological Institute (MNI) head (Evans et al., 1994). The head model was based on a three compartment realistic volume conductor and was used for the calculation of EEG forward solutions (Nolte and Dassios, 2005). The EMG signals were simulated for 10 different electrodes and the mixing matrix was random.

The sources of coherent activity were modelled as pseudo-random cortical dipoles. EEG oscillations were generated by band-pass filtering independent white noise in the 12–14 Hz and 24–26 Hz frequency ranges. Coherent EMG activities were modelled as a time-shifted version of the corresponding cortical oscillations. Therefore, the ground truth coherence without noise at the frequencies of interest was one.

For the generation of background EEG noise, we used 500 uncorrelated dipoles with random orientation and distribution on the cortex. The noise sources had $1/f$ type spectra. For the generation of background EMG noise we used 10 noise sources of random Gaussian noise randomly mixed with the signal sources. As a result we obtained activity from 10 simulated EMG sensors.

The simulated data was 300-s long and sampled at 200 Hz. In the first test the SNR of the CMC sources was 0.1 for EEG and 0.5 for EMG. In the second test the SNR of EEG signals was 0.01. For the EEG signals, the SNR was calculated as the ratio between the mean variance across channels for the projected sources and the mean variance of additive $1/f$ noise (produced by all noise dipoles) in the center frequency of the coherent source. The computation was similar for EMG, but the noise had uniform

spectrum.

For each recovered source, the error between the original pattern and the pattern recovered by caCOH was calculated according to:

$$Err = 1 - \frac{|a_o^T a_r|}{||a_o|| \cdot ||a_r||} \quad (16)$$

where a_o is the original simulated pattern and a_r is a pattern recovered by caCOH. The total error for all sources was obtained averaging over all errors.

This procedure was repeated 100 times with randomly located sources at each frequency.

2.3.1. Significance of coherence

The confidence limit (CL) for the coherence obtained with caCOH was computed using permutation tests (Hesterberg et al., 2005). For this procedure we repeated all steps of caCOH, but the EMG segments were shuffled with respect to the EEG data. For each permutation, we obtained a specific coherence value and altogether 500 permutations were performed, which corresponds to a p-value of 0.0224, see (Ojala and Garriga, 2010). We chose this value because it allows finding significant results and simultaneously maintaining a reasonably low computational cost. Thus, significant CMC values of the original data were those exceeding the 97.5 percentile of permuted coherence.

2.4. Dataset 1: low number of EMG channels

Data were recorded from 14 healthy volunteers without history of neurological or psychiatric disorders. The experimental protocol was approved by the Institutional Review Board of Charité, Berlin, and participants gave their written informed consent prior to the recordings. All subjects were right-handed according to the Edinburg Handedness Inventory (Oldfield, 1971) and had normal or corrected to normal vision. These data were already described in (Bayraktaroglu et al., 2011).

2.4.1. Paradigm

A digit displacement paradigm was used, where the participants had to manipulate a compliant object by moving a lever against a load and then maintaining a constant force. This paradigm was selected as previous studies reported that the coherence was greater when the task involved a compliant lever (Kilner et al., 2000b; Riddle and Baker, 2005a). Volunteers were seated in a comfortable chair with their arms rested on the chair handles, forearms flexed at 60 ° and hands pronated. Participants had to press a spring-loaded lever with the left or right thumb at 0.5 N force. The force level was measured with a Honeywell Load Sensor (FSG15N1A) and visually presented to the participants as a horizontal bar proportional to the exerted force. A cross in the center of the screen was also displayed and served as eye-fixation point. The displacement of the spring-loaded lever was 3.5 cm. Participants had to perform the task with each hand separately and the order was counter-balanced between participants. Participants were instructed to reach the desired force level as fast as possible after a single tone was presented and hold the force constant until a double tone was presented. One hundred trials were recorded for each hand in four blocks. Each trial lasted 9 s in total (5 s active and 4 s rest). There were 60 s of rest between the blocks.

2.4.2. Data acquisition

A BrainAmp MR plus from Brain Products (Germany) was used to record EEG and EMG data. The signals were filtered between 0.015 and 250 Hz with a voltage resolution of 0.1 μV for EEG and 0.5 μV for EMG. The sampling frequency as 1000 Hz but the data was later band pass filtered and downsampled to 200 Hz. The EEG data was referenced to physically linked earlobes. An EEG cap (EasyCapTM) with 61 Ag/AgCl sintered ring electrodes (12 mm diameter, EasyCap GmbH, Germany) densely covering the sensorimotor cortex was employed to record EEG signals. EOG signals were also acquired with two electrodes placed on the right zygomatic and supraorbital processes in order to asses ocular artifacts. Also EMG signals were acquired. In particular, 6 EMG electrodes were placed over the thenar side of each hand and signals were recorded from the Abductor Pollicis Brevis (APB) muscle. These electrodes were Ag/AgCl sintered sensors with 4 mm diameter. The EMG reference electrode was placed on the styloid process of the ulnar bone and a ground electrode on the inner surface of wrist at the midline, with Ag/AgCl sintered sensors of 12 mm diameter. Please, see the video of the paradigm provided as supplementary material, where a subject is siting relaxed with a thumb on a spring-loaded lever. Upon a presentation of an auditory beep, the subject presses on the lever reaching a force of about 0.5 N, this force being displayed on a screen as a horizontal bar proportional to the applied force.

2.5. Dataset 2: high-density EMG recordings

Data were recorded from 16 healthy volunteers without history of neurological or psychiatric disorders. The experimental protocol was approved by the Ethics Committee at the Faculty of Human Movement Sciences, Vrije Universiteit Amsterdam, and participants gave their written informed consent prior to the recordings. Two right-handed participants were selected for this study. The original data was published in de Vries et al. (2016).

2.5.1. Paradigm

Participants performed a bimanual precision-grip task during simultaneous recording of EEG and EMG signals. The participants held a compliant force sensor in each hand and had to produce force using a pinch grip. The subjects' task was to track a visual target by moving the cursor displayed on a monitor. At the start of each trial, the target was in the starting position. Then, it linearly moved to the final target position (force ramp) during the first 5 s, where it remained for 10 s (constant force). Participants moved the cursor by applying force to both sensors (left and right hand) with the aim of keeping the cursor within the target. The position of the cursor was a linear combination (weighting) of left and right forces generated by the participant, see de Vries et al. (2016) Fig. 1, for more details.

2.5.2. Data acquisition

EEG and high-density surface electromyography (HDsEMG) were recorded from all participants. EEG was acquired using a 64-electrode cap with electrodes placed according to the extended 10–20 system. Brain signals were amplified using a 64-channel Refa amplifier (sampling rate 1024 Hz; TMSi, Enschede, The Netherlands). HDsEMG was acquired using 2 64-channel (8x8, 4-mm interelectrode distance) electrode grids and amplified using a 128-channel Refa amplifier (sampling rate 2.048 Hz; TMSi). The electrode grids were placed over the flexor pollicis brevis (FPB) muscle of each hand. These data were synchronized using a trigger pulse sent to both amplifiers at the beginning of each trial.

2.6. Preprocessing

The data analysis was performed in MATLAB (2017a; The MathWorks, Natick, MA) using the BBCI toolbox (Blankertz et al., 2016), the Fieldtrip toolbox (Oostenveld et al., 2011), the EEGlab toolbox (Delorme and Makeig, 2004) and custom programmed software. All data were down-sampled to 200 Hz.

2.6.1. Dataset 1

CMC was estimated during the post-stimulus interval between 2 and 5 s, which corresponded to the stable hold period of the task. This is the interval at which the strongest coherent activity in beta band can be expected (Baker et al., 1997; Kristeva et al., 2007; Riddle and Baker, 2005a). Before CMC calculation, artefactual trials were rejected by visual inspection for the presence of strong abrupt force changes in the hold

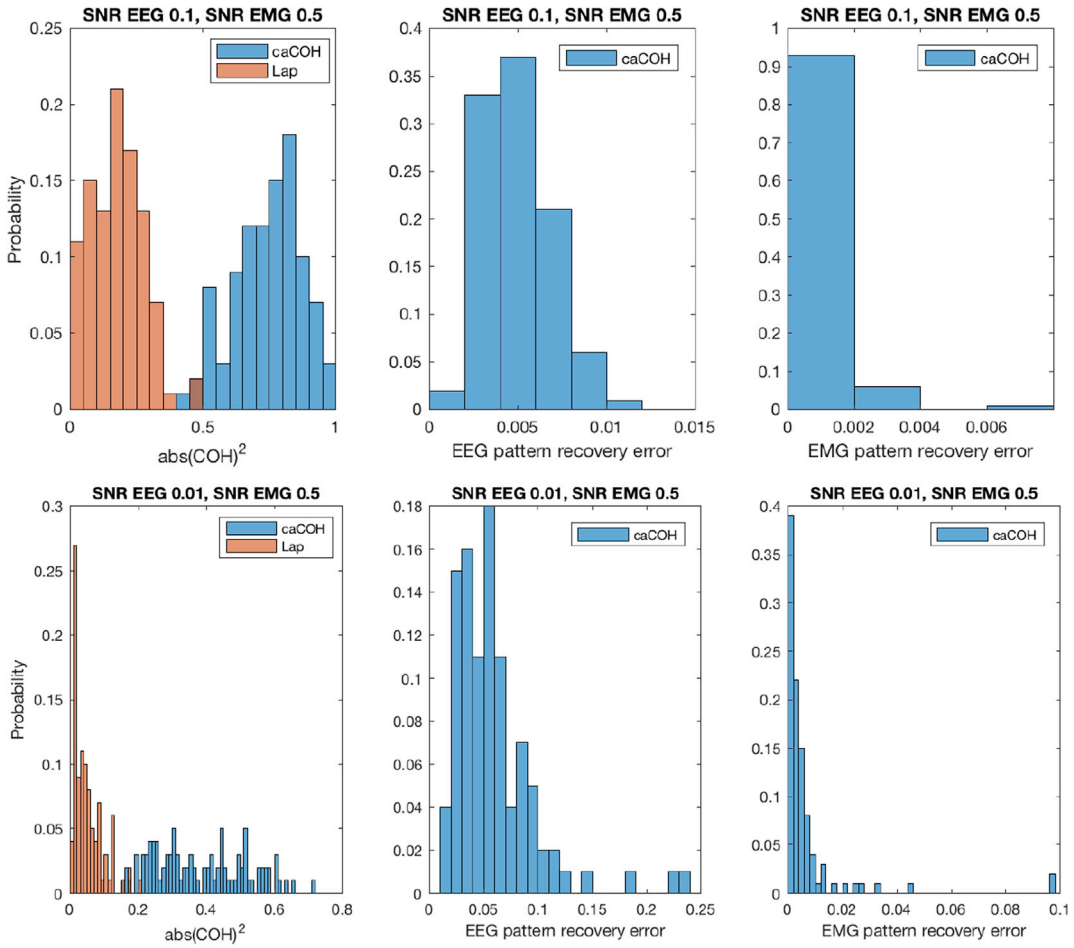

Fig. 1. Results of the simulations. Left: histogram of CMC strength values for caCOH (blue) and Laplacian channels (orange). Center: histogram of pattern recovery errors for EEG signals. Right: histogram of pattern recovery errors for EMG signals. Note that recovery errors can only be computed for caCOH and not for Laplacian channels. Up: SNR_{EEG} is 0.1. Bottom: SNR_{EEG} is 0.01.

period. If the force output deviated from 0.5 ± 0.1 N range, the epoch was discarded, (see Bayraktaroglu et al. (2011)).

2.6.2. Dataset 2

CMC was estimated during the post-stimulus interval between 6 and 15 s, which again corresponded to the constant force task. Before CMC calculation, artefactual EEG and EMG channels were manually rejected based on their variance in the band range between 8 and 30 Hz. Additionally, ICA was applied to EEG data to further remove artefactual components. Redundancy of EMG data was reduced by applying Principal Component Analysis (PCA) on the EMG band-pass filtered data between 10 and 28 Hz. The number of dimensions maintained corresponded to 99% of the variance.

3. Results

3.1. Simulations

Fig. 1 shows the simulation results. They represent the CMC strength and error of EEG and EMG pattern recovery in the simulated conditions. The left panel of this Figure shows that the CMC strength is significantly higher for caCOH in comparison to Laplacian channels in both SNR_{EEG} conditions ($p << 0.01$ for both frequencies using Wilcoxon tests). In the case of low SNR (i.e. $SNR_{EEG} = 0.01$) the average CMC strength was 0.38 for caCOH and 0.05 for Laplacian derviations after 100 repetitions. Additionally, the center and right panels of Fig. 1 depict histograms of errors found in the recovery of EEG and EMG patterns of caCOH. The recovery errors are very small, concentrated around 0.005 for EEG and 0.001 for EMG if $SNR_{EEG} = 0.1$ and around 0.05 for EEG and 0.001 for EMG if $SNR_{EEG} = 0.01$\$, which indicates a very good performance of the caCOH algorithm, even under very low SNR conditions.

Fig. 2 provides an example of pattern recovery and CMC strength obtained with caCOH. Note that the algorithm recovers both EEG sources that are active simultaneously at different frequencies. Importantly, caCOH correctly recovers patterns of EEG and EMG sources. Note here that it is not possible to recover patterns of sources using Laplacian derivations. At the bottom of Fig. 2 we also show the result of an additional experiment where EEG signals had a very low SNR of 0.01. This plot shows that in this condition Laplacian derivations cannot recover CMC but caCOH delivers the expected peaks at the frequency bands of interest.

3.2. Dataset 1: grand-average caCOH

The subjects were able to keep the required force level during the active period of the trials. The trials exceeding ± 0.1 N of the desired force in the analyzed period (2–5 s), were removed from the analysis. The left panel of Fig. 3 shows the averaged patterns of left (up) and right hand (down) chosen at the maximum caCOH frequency bin. The mean frequency and standard error of CMC for the left and right hand performance was 20.3 ± 1.5 and 18.3 ± 1.6 Hz, respectively. In order to correctly average patterns we computed the correlation between the

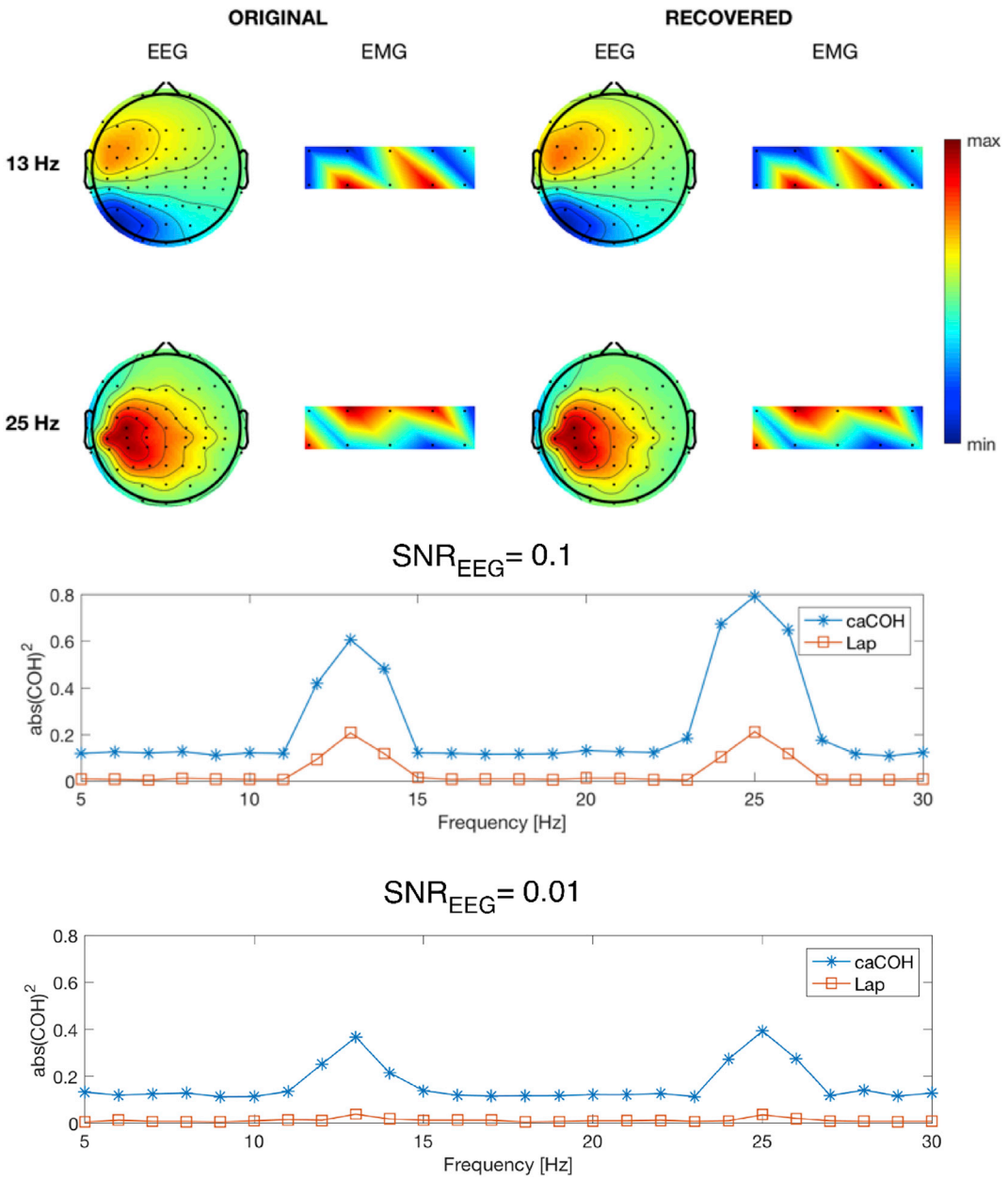

Fig. 2. Example of the pattern recovery in simulations. Up Left: original EEG and EMG patterns at two different frequencies. Up Right: recovered EEG and EMG patterns at two different frequencies. Middle: caCOH and Laplacian CMC spectrum with SNR_{EEG} at 0.1. Bottom: caCOH and Laplacian CMC spectrum under low SNR conditions, SNR_{EEG} at 0.01. Note that ground truth CMC is 1 at the frequencies of interest.

pattern of one subject to all the patterns from other subjects and corrected the sign if the correlation was negative in order to stratify the polarity of the sources.

We also calculated the cortical sources corresponding to the patterns of sources obtained with caCOH, shown in the left panel of Fig. 3. The inverse modelling was performed with eLORETA (Pascual-Marqui et al., 2011). The right panel of Fig. 3 shows corresponding eLORETA solutions. The active sources were primarily localized over the contralateral pre- and post-central gyri.

3.3. Dataset 1: within-subject specificity

Fig. 4 shows further advantages of the caCOH method with respect to resolving CMC at different frequency ranges. It demonstrates optimized patterns at each frequency bin (top of figure) and a spectrum of optimized CMC (bottom). Here it is important to show data from a single participant since the location of the peaks in CMC varies across participants. At the bottom of Fig. 4 one can observe the optimized CMC spectrum where red stars indicate a significant result after permutation testing. In general, one can see that, although the patterns at different frequency ranges correspond mostly to sources located in the sensorimotor areas of the right and left hemisphere, there are also small variations in the spatial features thus making each pattern unique in its relation to the underlying neuronal source. The patterns whose scalp is circled in magenta were selected to perform eLORETA source localization. A spatial distribution of these sources confirms further a heterogeneity of the neuronal activity underlying CMC at different peak frequencies as could be seen in Fig. 5. Finally, the maximal CMC values using common average reference signals were 0.065 and 0.077 for left and right hand respectively, using Laplacian derivations these values were 0.088 and 0.210 and for caCOH they were 0.202 and 0.225.

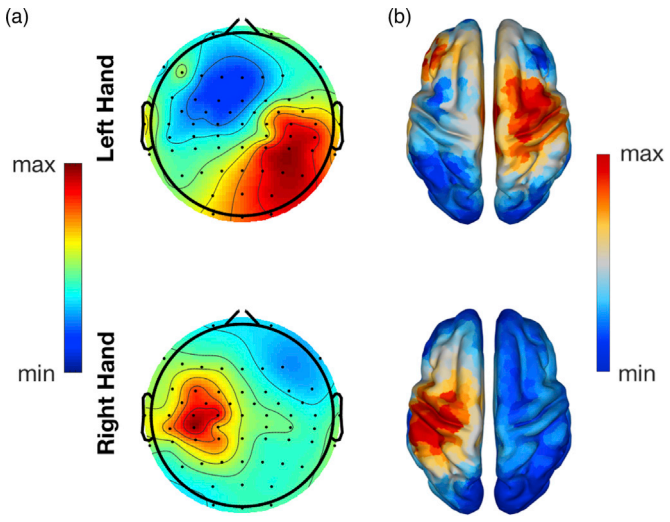

Fig. 3. Patterns and sources for CMC obtained in the first dataset from the grand-average of subjects. Red color indicates stronger sources, whereas blue color means weaker sources. (a) Averaged caCOH patterns for left (up) and right hand (down) at the maximal CMC frequency of each subject. (b) eLORETA source localization of patterns shown on the left panel.

3.4. Dataset 2: inter-subject specificity

For illustrative purposes we selected data from two participants where EMG was recorded using high-density electrode grids (see Methods). This allowed us to calculate and visualize not only spatial patterns of EEG but also of EMG activity. In Fig. 6 it is possible to observe distinct patterns at different frequencies for both the EEG and EMG signals. On the bottom one can see the optimized CMC spectrum. Red dots indicate that the result is significant, magenta circles indicate the frequency of the EEG and EMG patterns selected for visualization on the top of each CMC spectrum.

The maximal CMC values obtained with common average reference signals were 0.120 and 0.178 for Subject 1 (respectively left and right hand), with Laplacian derivations those values were 0.145 and 0.206 and for caCOH they were 0.299 and 0.321. For Subject 2 and common average reference signals the coherence values were 0.246 and 0.085, for Laplacian derivations the results were 0.264 and 0.120, and finally they were 0.362 and 0.237 for caCOH.

For the subjects in Fig. 6 we also localized the EEG patterns at the frequencies circled in magenta in that figure. The results are shown in Fig. 7. In this case of bilateral hand performance, we observe neuronal sources primarily over the contralateral sensorimotor cortices with respect to the EMG from the hand used for caCMC. Yet, occasionally we also detect bilateral patterns of neuronal activation over the sensorimotor areas, e.g. in Subject 1, right hand.

4. Discussion

Here we presented a novel method to maximize CMC between two multivariate spaces called caCOH. It is based on the maximization of the absolute value of the coherence in the frequency domain. For each frequency bin, two spatial filters are computed in order to maximize the coherence between the projected components. When applied to EEG and EMG, one obtains a maximization of CMC with individual spatial patterns for cortical and muscle activity.

4.1. Maximization of coherence with caCOH

caCOH finds a linear combination of all EEG and all EMG electrodes that maximizes the absolute value of coherence between both signals. The fact that all EEG and all EMG channels can be used distinguishes this method from other CMC estimates based on bipolar or Laplacian filtering. caCOH presents also advantages over rCMC (Bayraktaroglu et al., 2011), which is based on multiple regression and that can only be applied to a single EMG channel and specific frequency bands. In the case

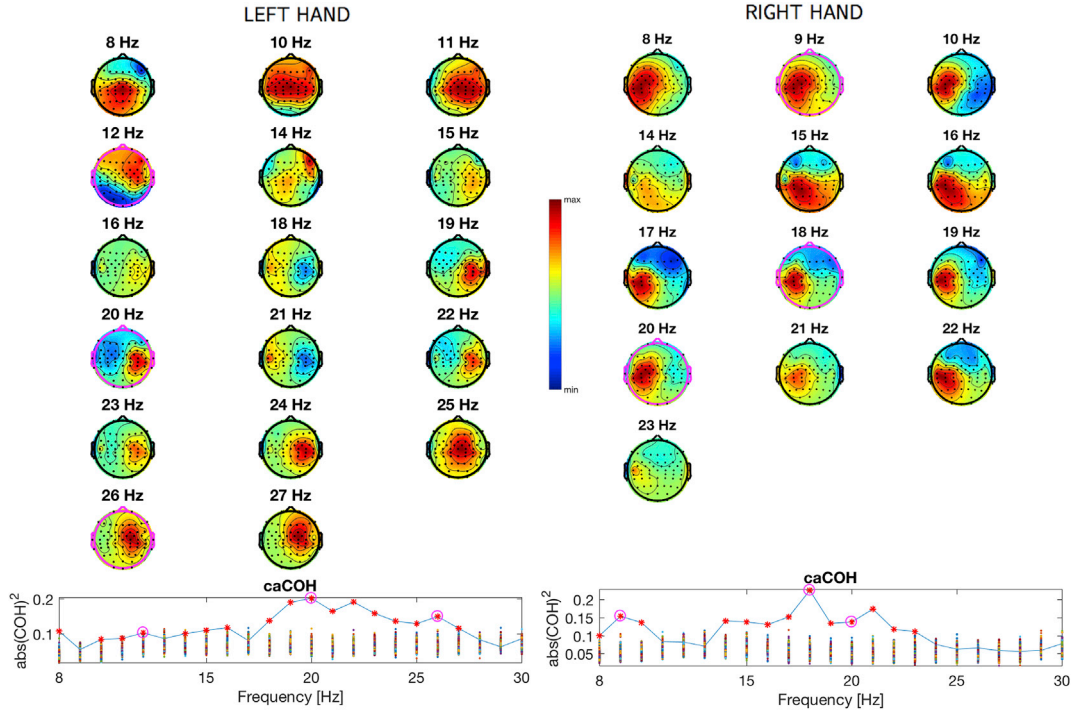

Fig. 4. CMC topographies and spectra for a representative subject. Top: EEG patterns found with caCOH of a single subject. Bottom: spectrum of caCOH strength. Patterns marked in magenta were selected for localization. Small vertical lines at each frequency bin consisting of dots indicate permutation runs. Points on CMC spectra, lying above these vertical bars, indicate significant phase synchronization between EEG and EMG activity.

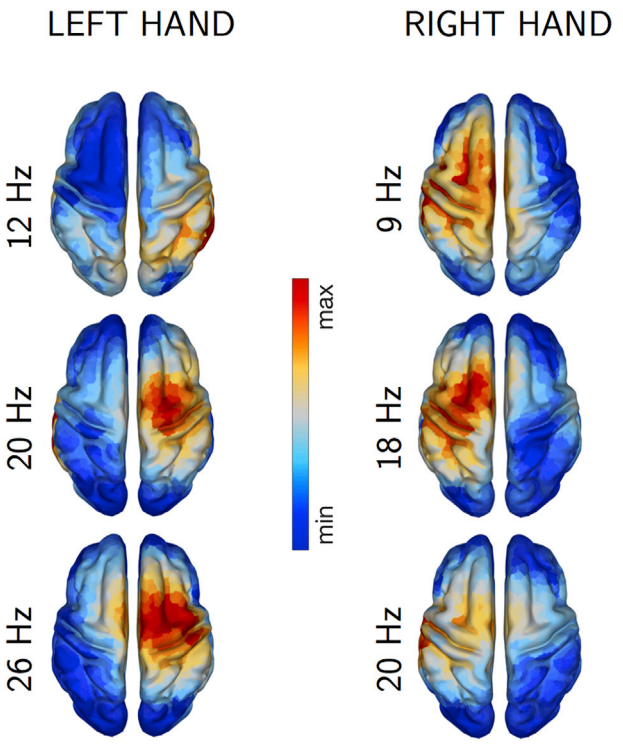

Fig. 5. eLORETA solution for CMC patterns shown in Fig. 4. The patterns were obtained from a representative subject. On the left column one can see the results of the localization of patterns found for the left hand, respectively on the right column patterns of the right hand are visible. The frequencies at which the patterns were obtained are also displayed next to the respective pictures. Red color indicates stronger sources whereas blue color means weaker sources.

of caCOH, the maximization is iteratively performed for all frequency bins and delays. Thus, caCOH can be used to explore CMC subject-dependent peaks and patterns over the complete frequency range of interest.

Additionally, and unlike coherence estimation based on Laplacian derivations, caCOH allows the recovery of both EEG and EMG topographies related to cortical and muscular coherent sources. Thus, it is possible to reconstruct neuronal sources coupled with maximum coherence using inverse modelling (such as the eLORETA method). These inverse solutions showed that caCOH topographies were best modelled by sources in the contralateral sensorimotor areas, in agreement with previous studies (Gross et al., 2001; Salenius et al., 1997; Schoffelen et al., 2008).

caCOH exhibits several advantages over single channel approaches to compute CMC (Yao et al., 2007). These methods suffer from major mixing of signals from multiple oscillatory sources, which represents a serious drawback to study activity from specific cortical areas. Other approaches employing spatial filters, such as bipolar (Graziadio et al., 2010) or Laplacian derivations (Mima and Hallett, 1999) can alleviate the superposition problem, but do not take into account EMG information, and they could filter out neuronal oscillations that effectively contribute to CMC. Beamformer techniques have proved useful to study CMC (Gross et al., 2001; Schoffelen et al., 2008) but require massive statistical testing for each voxel and the use of detailed conductivity information that is not always available.

4.2. Simulations

Results of the simulations in Fig. 1 show that caCOH is able to accurately extract CMC values and recover EEG and EMG patterns occurring simultaneously at two different frequencies. Moreover, caCOH estimated significantly higher CMC in comparison to Laplacian channels. When the SNR was very low, Laplacian channels recovered CMC values barely over 0, whereas caCOH could recover peaks of around 0.38 in

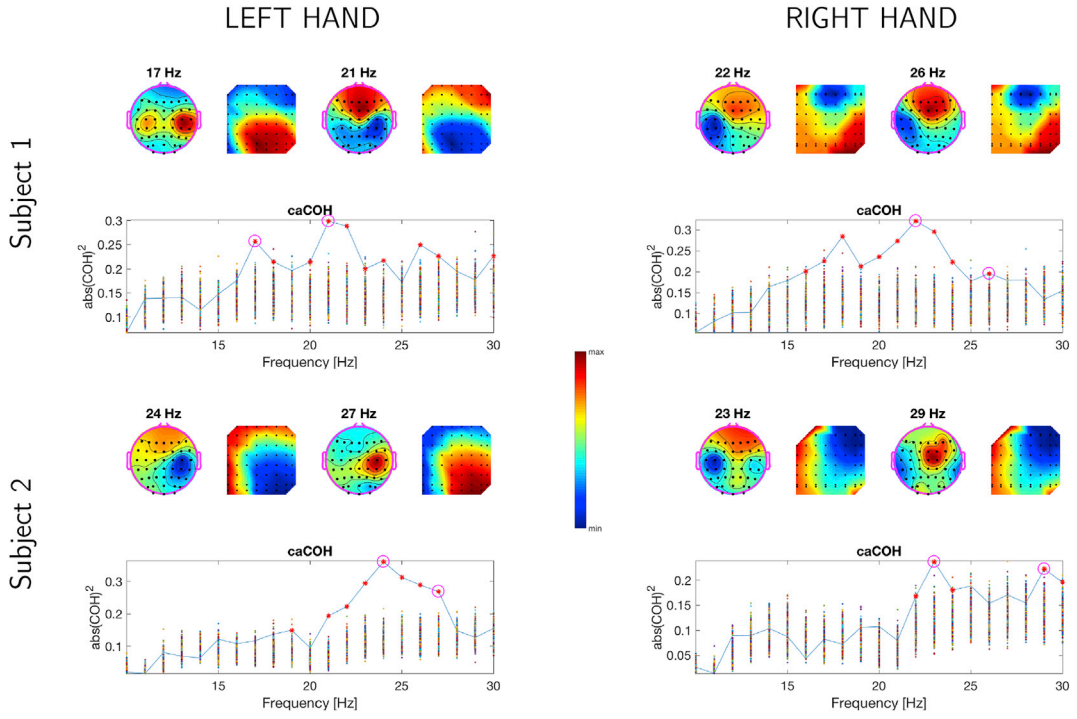

Fig. 6. Examples of individual EEG and EMG topographies obtained with caCOH. Top: EEG and EMG patterns optimizing CMC of a single subject at specific frequency bins. Bottom: spectrum of caCOH strength.

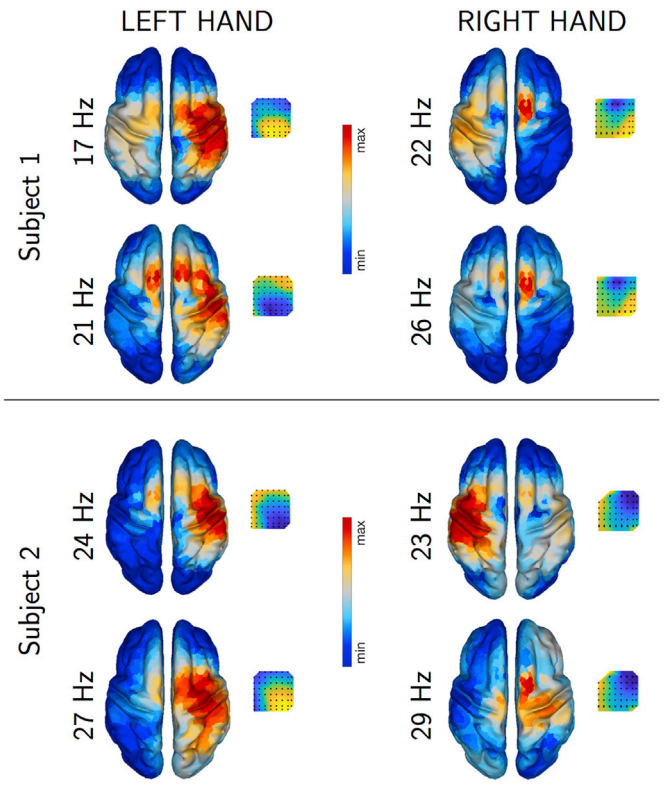

Fig. 7. Localization of coherent activity representing inter-subject variability of CMC results. Sources are obtained with eLORETA, for two subjects at the frequency bins shown in Fig. 6. Their corresponding EMG patterns are on the right of each source figure. Red color indicates stronger sources and blue color whereas blue color means weaker sources.

average. Thus, caCOH was still able to recover CMC peaks where Laplacian derivations did not show clear CMC. This is due to the fact that caCOH spatial filters not only reflect the configuration of sources but also project out noise contributions distributed among 500 dipoles generating $1/f$ noise. In addition, and as shown in section 3.1, the recovery error for EEG and EMG patterns was very small even for very low SNRs.

Furthermore, as caCOH operates iteratively over all frequency bins, it is possible to recover patterns and components for different oscillatory components, as demonstrated in Fig. 2. Again, this figure shows that caCOH has stronger values compared to Laplacian channels, which is particularly important for the signals with poor SNR. In fact, in many papers reporting CMC research one can see rather flat coherence spectra with only some hints of the peaks. The use of caCOH would guarantee the best multivariate solution for the spatial filter, thus providing a higher sensitivity for the detection of interactions between cortical and muscle activity. Finally, in our simulations (Fig. 2) it is possible to see that the lowest levels of CMC are higher for caCOH (between 0.10 and 0.15) than for Laplacian derivations. This is due to the optimization, that causes overfit at the frequency bins where CMC is not present. Thus, in order to obtain significant CMC values, one needs to run permutation tests as explained in Section 2.3.1.

4.3. Subject-specific results

As shown in Section 3, caCOH provides a CMC spectrum for all frequency bins. The subject-specific results reveal peaks at several frequencies corresponding to μ and β bands. Moreover, the peaks and patterns of maximal CMC are subject-dependent. Furthermore, there usually exist several frequency bins where CMC is significant according to the permutation tests. Yet, these peaks do not occur at the same frequencies in different subjects. The results for the first dataset clearly demonstrate contralateral neuronal sources that are particularly pronounced in the precentral gyrus. In our case, we performed inverse source modelling of caCOH patterns with eLORETA. Nevertheless, these patterns can also be used for inverse modelling with equivalent current dipoles, minimum-norm estimates and beamformers. The time courses of caCOH, however, directly represent source activity. And thus one can investigate their temporal dynamics using phase and amplitude.

An example of different patterns at different frequency bins for the same subject is shown in Figs. 4 and 5. It can be seen that patterns and their corresponding sources depend on the frequency bin at which they are measured. Even, CMC values of different hands are not necessarily significant at the same frequency bins for the same subject. The dissimilarity between patterns can be quantified using a technique similar to the calculation of the recovery error (see Section 2.3). The larger the error, the higher the difference between patterns at different frequency bins. We computed these errors between those patterns circled in magenta in Fig. 4, the results ranged between 0.79 and 0.49 for the left hand and between 0.90 and 0.36 for the right hand. This in turn indicates a contribution of distinct neuronal CMC sources for different frequency bins. This is one of the aspects that up to now was difficult to assess, whereas this is now possible with caCOH.

An example of different patterns from different subjects is also visible in Fig. 6. In this case, caCOH can be used to its full advantage as we have multichannel high-density recordings for both cortical and muscle activity. The motor task in this paradigm required a simultaneous control with both hands, that can be associated with the bilateral activation of sensorimotor cortices (Fig. 7). This control is known to be associated with the activation of both hemispheres, not only in the primary motor cortex but also in pre-motor and supplementary motor cortices (Swinnen and Wenderoth, 2004; Noble et al., 2014). The presented findings show that caCOH is able to extract multiple distinct patterns of cortico-muscular interactions between different cortical and spinal regions involved in bimanual motor performance.

4.4. caCOH as a general tool for studying synchronization between simultaneously recorded datasets

caCOH is not limited to studying cortico-muscular interactions. There are also other scenarios in EEG/MEG/LFP research where this method can be utilized. caCOH can be used for the investigation of neuronal interactions between cortical (EEG/MEG) and subcortical activity, the latter is typically recorded as a result of neurosurgery relating to different neurological problems. For instance in Parkinson's Disease, electrodes can be implanted to the Subthalamic nucleus (STN) for the therapeutic purposes. A number of previous studies investigated interactions between cortical MEG activity and STN activity reflected in STN LFPs (Litvak et al., 2010). In those studies, however, cortico-STN coherence was calculated using different combinations of each STN contact and cortical sensor or voxel activity (e.g. after beamforming) obtained with MEG. In our case, one can apply caCOH to find simultaneous spatial projections for two datasets representing subcortical and cortical activity. Another example for the use of caCOH is hyperscanning, where EEG activity is simultaneously recorded from two (or even more) subjects (Koike et al., 2015). The rationale is to find synchronization between neuronal activity of two subjects. Instead of using mass-bivariate calculations of synchronization between homologous electrodes in both subjects, one could use caCOH to find spatial filters for each subject to identify neuronal activity that is maximally synchronous between subjects.

In conclusion, we have developed a novel method for phase synchrony detection based on the maximization of the absolute value of coherence between neural signals of different origins (for example brain and muscular signals) in the frequency domain. The method, called caCOH, was used in this work to maximize CMC by taking the complete

EEG and EMG spaces into account.caCOH also allowed the extraction of EEG and EMG topographies, that could be then used for an inverse localization of neuronal and muscular sources over the complete spectrum of interest. Importantly, caCOH allows subject-specific maximization of coherence over the complete frequency spectrum. Finally, the method can also be used for other studies relating to the investigation of cortico-subcortical interactions and neuronal synchronization between subjects in case of hyperscanning.

Acknowledgements

C.V. was supported by the Spanish Ministry of Economy with Grant RyC 2014-15671. G.N. was partially funded by the German Research Foundation (DFG, SFB936 Z3 and TRR169, B4). K.-R.M. work was supported by the German Ministry for Education and Research (BMBF) under Grants 01IS14013A-E, 01GQ1115 and 01GQ0850; the German Research Foundation (DFG) under Grant Math+, EXC 2046/1, Project ID 390685689 and by the Institute for Information & Communications Technology Planning & Evaluation (IITP) grant funded by the Korea government (No. 2017-0-00451, No. 2017-0-01779). T.W.B. was supported by a Future Fellowship from the Australian Research Council (FT180100622). V.V.N. was partially supported by the Center for Bioelectric Interfaces NRU HSE, RF Government grant, ag. No. 14.641.31.0003. The authors thank Katherina von Carlowitz-Ghori for her support with rCMC code and results.

Appendix A. Supplementary data

Supplementary data to this article can be found online at https://doi.org/10.1016/j.neuroimage.2019.116009.

References

Andrykiewicz, A., Patino, L., Naranjo, J.R., Witte, M., Hepp-Reymond, M.-C., Kristeva, R., 2007. Corticomuscular synchronization with small and large dynamic force output. BMC Neurosci. 8, 101.

Baker, M.R., Baker, S.N., 2002. The effect of diazepam on motor cortical oscillations and corticomuscular coherence studied in man. J. Physiol. 546 (3), 931–942.

Baker, S.N., 2007. Oscillatory interactions between sensorimotor cortex and the periphery. Curr. Opin. Neurobiol. 17 (6), 649–655.

Baker, S.N., Olivier, E., Lemon, R.N., 1997. Coherent oscillations in monkey motor cortex and hand muscle emg show task-dependent modulation. J. Physiol. 501 (1), 225–241.

Bayraktaroglu, Z., von Carlowitz-Ghori, K., Losch, F., Nolte, G., Curio, G., Nikulin, V.V., 2011. Optimal imaging of cortico-muscular coherence through a novel regression technique based on multi-channel eeg and un-rectified emg. Neuroimage 57, 1059–1067.

Bießmann, F., Meinecke, F.C., Gretton, A., Rauch, A., Rainer, G., Logothetis, N.K., Müller, K.-R., 2010. Temporal kernel cca and its application in multimodal neuronal data analysis. Mach. Learn. 79 (1), 5–27.

Bießmann, F., Plis, S., Meinecke, F., Eichele, T., Müller, K.-R., 2011. Analysis of multimodal neuroimaging data. IEEE Reviews in Biomedical Engineering 4, 26–58.

Blankertz, B., Acqualagna, L., Dähne, S., Haufe, S., Schultze-Kraft, M., Sturm, I., Uscumlic, M., Wenzel, M., Curio, G., Müller, K., 2016. The berlin brain-computer interface: progress beyond communication and control. Front. Neurosci. 10.

Calhoun, V., Liu, J., Adali, T., 2009. A review of group ica for fMRI data and ica for joint inference of imaging, genetic, and erp data. Neuroimage 45 (1), 163–172.

Conway, B.A., Halliday, D.M., Farmer, S.F., Shahani, U., Maas, P., Weir, A.I., Rosenberg, J.R., 1995. Synchronization between motor cortex and spinal motoneuronal pool during the performance of a maintained motor task in man. J. Physiol. 489 (3), 917–924.

Dähne, S., Biessmann, F., Samek, W., Haufe, S., Goltz, D., Gundlach, C., Villringer, A., Fazli, S., Müller, K.-R., 2015. Multivariate machine learning methods for fusing multimodal functional neuroimaging data. Proc. IEEE 109, 1507–1530.

de Vries, I.E.J., Daffertshofer, A., Stegeman, D.F., Boonstra, T.W., 2016. Functional connectivity in the neuromuscular system underlying bimanual coordination. J. Neurophysiol. 116, 2576–2585.

Delorme, A., Makeig, S., 2004. EEGLAB: an open source toolbox for analysis of single-trial eeg dynamics. J. Neurosci. Methods 134, 9–21.

Donoghue, J.P., Sanes, J.N., Hatsopoulos, N.G., Gaál, G., 1998. Neural discharge and local field potential oscillations in primate motor cortex during voluntary movements. J. Neurophysiol. 79 (1), 159–173.

Engel, A.K., Roelfsema, P.R., Fries, P., Brecht, M., Singer, W., 1997. Role of the temporal domain for response selection and perceptual binding. Cerebr. Cortex 7 (6), 571–582.

Evans, A.C., Kamber, M., Collins, D.L., MacDonald, D., 1994. An mri-based probabilistic atlas of neuroanatomy. In: Shorvon, S.D., Fish, D.R., Andermann, F., Bydder, G.M., Stefan, H. (Eds.), Magnetic Resonance Scanning and Epilepsy. Springer US, Boston, MA, pp. 263–274.

Fries, P., 2005. A mechanism for cognitive dynamics: neuronal communication through neuronal coherence. Trends Cogn. Sci. 9 (10), 474–480.

Graziadio, S., Basu, A., Tomasevic, L., Zappasodi, F., Tecchio, F., Eyre, J.A., 2010. Developmental tuning and decay in senescence of oscillations linking the corticospinal system. J. Neurosci. 30 (10), 3663–3674.

Gross, J., Kujala, J., Hämäläinen, M., Timmermann, L., Schnitzler, A., Salmelin, R., 2001. Dynamic imaging of coherent sources: studying neural interactions in the human brain. Proc. Natl. Acad. Sci. 98 (2), 694–699.

Halliday, D.M., Conway, B.A., Farmer, S.F., Rosenberg, J.R., 1998. Using electroencephalography to study functional coupling between cortical activity and electromyograms during voluntary contractions in humans. Neurosci. Lett. 241 (1), 5–8.

Hesterberg, T., Moore, D., Monaghan, S., Clipson, A., Epstein, R., 2005. Bootstrap methods and permutation tests. In: Moore, D., McCabe, G. (Eds.), Introduction to the Practice of Statistics. W.H. Freeman, New York, pp. 14.1–14.70.

Jackson, A., Spinks, R.L., Freeman, T.C.B., Wolpert, D.M., Lemon, R.N., 2002. Rhythm generation in monkey motor cortex explored using pyramidal tract stimulation. J. Physiol. 541 (3), 685–699.

Kilner, J.M., Baker, S.N., Salenius, S., Hari, R., Lemon, R.N., 2000a. Human cortical muscle coherence is directly related to specific motor parameters. J. Neurosci. 20 (23), 8836–8845.

Kilner, J.M., Baker, S.N., Salenius, S., Hari, R., Lemon, R.N., 2000b. Human cortical muscle coherence is directly related to specific motor parameters. J. Neurosci. 20 (23), 8838–8845.

Koike, T., Tanabe, H., Sadato, N., 2015. Hyperscanning neuroimaging technique to reveal the "two-in-one" system in social interactions. Neurosci. Res. 90, 25–32.

Kristeva, R., Patino, L., Omlor, W., 2007. Beta-range cortical motor spectral power and corticomuscular coherence as a mechanism for effective corticospinal interaction during steady-state motor output. Neuroimage 36 (3), 785–792.

Kristeva-Feige, R., Fritsch, C., Timmer, J., Lücking, C.-H., 2002. Effects of attention and precision of exerted force on beta range eeg–emg synchronization during a maintained motor contraction task. Clin. Neurophysiol. 113 (1), 124–131.

Litvak, V., amd, A., Jha, A.E., Oostenveld, R., Barnes, G., Penny, W., Zrinzo, L., Hariz, M., Limousin, P., Friston, K., Brown, P., 2010. Optimized beamforming for simultaneous meg and intracranial local field potential recordings in deep brain stimulation patients. Neuroimage 50 (4), 1578–1580.

Mima, T., Hallett, M., 1999. Electroencephalographic analysis of cortico-muscular coherence: reference effect, volume conduction and generator mechanism. Clin. Neurophysiol. 110 (11), 1892–1899.

Murthy, V.N., Fetz, E.E., 1992. Coherent 25- to 35-hz oscillations in the sensorimotor cortex of awake behaving monkeys. Proc. Natl. Acad. Sci. 89 (12), 5670–5674.

Noble, J., Eng, J., Boyd, L., 2014. Bilateral motor tasks involve more brain regions and higher neural activation than unilateral tasks: an fmri study. Exp. Brain Res. 232 (9), 2785–2795.

Nolte, G., Dassios, G., 2005. Analytic expansion of the eeg lead field for realistic volume conductors. Phys. Med. Biol. 50, 3807–3823.

Ojala, M., Garriga, G.C., 2010. Permutation tests for studying classifier performance. JMLR 11, 1833–1863.

Oldfield, R.C., 1971. The assessment and analysis of handedness: the edinburgh inventory. Neuropsychologia 9 (1), 97–113.

Oostenveld, R., Fries, P., Maris, E., Schoffelen, J.-M., 2011. Fieldtrip: open source software for advanced analysis of MEG, EEG, and invasive electrophysiological data. Comput. Intell. Neurosci. 2011, 156869.

Pascual-Marqui, R.D., Lehmann, D., Koukkou, M., Kochi, K., Anderer, P., Saletu, B., Tanaka, H., Hirata, K., John, E., Prichep, L., Biscay-Lirio, R., Kinoshita, T., 2011. Assessing interactions in the brain with exact low-resolution electromagnetic tomography. Philos Trans A Math Phys Eng Sci 369 (1952), 3768–3784.

Penfield, W., 1954. Mechanisms of voluntary movement. Brain 77 (1), 1–17.

Riddle, C.N., Baker, S.N., 2005a. Manipulation of peripheral neural feedback loops alters human corticomuscular coherence. J. Physiol. 566 (2), 625–639.

Riddle, C.N., Baker, S.N., 2005b. Manipulation of peripheral neural feedback loops alters human corticomuscular coherence. J. Physiol. 566 (2), 625–639.

Saglam, M., Matsunaga, K., Murayama, N., Hayashida, Y., Huang, Y.Z., Nakanishi, R., 2008. Parallel inhibition of cortico-muscular synchronization and cortico-spinal excitability by theta burst tms in humans. Clin. Neurophysiol. 119 (12), 2829–2838.

Salenius, S., Hari, R., 2003. Synchronous cortical oscillatory activity during motor action. Curr. Opin. Neurobiol. 13 (6), 678–684.

Salenius, S., Portin, K., Kajola, M., Salmelin, R., Hari, R., 1997. Cortical control of human motoneuron firing during isometric contraction. J. Neurophysiol. 77 (6), 3401–3405.

Schnitzler, A., Gross, J., Timmermann, L., 2000. Synchronised oscillations of the human sensorimotor cortex. Acta Neurobiol 60 (2), 271–287.

Schoffelen, J.-M., Oostenveld, R., Fries, P., 2005. Neuronal coherence as a mechanism of effective corticospinal interaction. Science 308 (5718), 111–113.

Schoffelen, J.-M., Oostenveld, R., Fries, P., 2008. Imaging the human motor system's beta-band synchronization during isometric contraction. Neuroimage 41 (2), 437–447.

Steeg, C., Daffertshofer, A., Stegeman, D., Boonstra, T., 2014. High-density surface electromyography improves the identification of oscillatory synaptic inputs to motoneurons. J. Appl. Physiol. 116 (10), 1263–1271.

Swinnen, S., Wenderoth, N., 2004. Two hands, one brain: cognitive neuroscience of bimanual skill. Trends Cogn. Sci. 8, 18–25.
Tsujimoto, T., Mima, T., Shimazu, H., Isomura, Y., 2009. Directional organization of sensorimotor oscillatory activity related to the electromyogram in the monkey. Clin. Neurophysiol. 120 (6), 1168–1173.
Varela, F., Lachaux, J.P., Rodriguez, E., Martinerie, J., 2001. The brainweb: phase synchronization and large-scale integration. Nat. Rev. Neurosci. 2 (4), 229–239.
Witham, C.L., Wang, M., Baker, S.N., Nelson, R.J., 2010. Corticomuscular coherence between motor cortex, somatosensory areas and forearm muscles in the monkey. Neuroscience 4, 38.
Yao, B., Salenius, S., Yue, G., Brown, R., Liu, J., 2007. Effects of surface emg rectification on power and coherence analyses: an eeg and meg study. J. Neurosci. Methods 159 (2), 215–223.